


Quantum Rings Engineered by Atom Manipulation

Van Dong Pham,¹ Kiyoshi Kanisawa,² and Stefan Fölsch¹

¹*Paul-Drude-Institut für Festkörperelektronik, Hausvogteiplatz 5-7,*

Leibniz-Institut im Forschungsverbund Berlin e. V., 10117 Berlin, Germany

²*NTT Basic Research Laboratories, NTT Corporation, 3-1 Morinosato Wakamiya, Atsugi, Kanagawa 243-0198, Japan*

 (Received 25 April 2019; published 6 August 2019)

We created hexagonal rings on a semiconductor surface by atom manipulation in a scanning tunneling microscope (STM). Our measurements reveal the generic level structure of a quantum ring, including its single ground state and doubly degenerate excited states. The ring shape leads to a periodic potential modulation and thereby a perturbation of the level structure that can be understood in analogy to band gap formation in a one-dimensional periodic potential. The modulation can be enhanced or inverted by further adding or removing atoms with the STM tip. Our results demonstrate the possibility of designing and controlling electron dynamics in a tunable periodic potential, holding promise for the construction of two-dimensional artificial lattices on a semiconductor surface.

DOI: [10.1103/PhysRevLett.123.066801](https://doi.org/10.1103/PhysRevLett.123.066801)

Quantum rings enable phase-coherent electron motion along a closed path, offering the possibility to explore fundamental quantum phenomena like the Aharonov-Bohm effect [1–5], persistent currents [6–9], or many-body correlations [10]. They can also be employed for implementing logic gate function [11,12]. Quantum rings have been realized in semiconductor materials, for example, by growing quantum dots and transforming them to ringlike structures [13] or by depleting a two-dimensional electron gas using the electric field effect or local oxidation techniques [3–5,9,10]. In this Letter, we use atom manipulation [14] by cryogenic scanning tunneling microscopy (STM) to assemble individual atomic rings on a semiconductor surface. This approach is unique in the sense that it provides perfection in structure and the capability to modify it at the atomic level. It will be shown, first, that the assembled rings exhibit discrete electronic states that reflect the generic features of quantum confinement along a closed path [13,15]. Second, these states can be manipulated by locally modifying the confining potential. We experimentally demonstrate that a *periodic* modulation leads to states with an energy level structure and a wave function character that can be understood in analogy to electron behavior in a one-dimensional (1D) periodic potential. Our system opens up the possibility to design and control electron dynamics in an artificial lattice created on a semiconductor surface.

As a template for the creation of the quantum rings, we employed the InAs(111)A surface grown by molecular beam epitaxy (MBE); details on the growth procedure are given elsewhere [16]. All STM measurements were carried out at a sample temperature of 5 K. Scanning tunneling spectroscopy was used to probe the electronic density of states of the quantum rings by recording the differential tunnel conductance dI/dV . Conductance spectra were

acquired using lock-in technique with a peak-to-peak bias modulation of 5–10 mV. MBE-grown InAs(111)A hosts a low concentration (roughly 0.005 monolayer) of In adatoms adsorbed on the vacancy sites of the (2×2) -reconstructed surface [17]. These native adatoms are positively charged [18] and can be readily repositioned by the STM tip [19,20].

To illustrate the electronic structure of the quantum rings assembled on InAs(111)A, we start the discussion with a linear chain composed of 30 In adatoms as shown in the STM topography image in Fig. 1(a). The adatoms occupy vacancy sites along a $\langle 211 \rangle$ in-plane direction and are $\sqrt{3}a' = 14.84 \text{ \AA}$ apart, where $a' = 8.57 \text{ \AA}$ is the lattice constant of the 2×2 In-vacancy reconstruction. Because of the electrostatic potential induced by the positively charged adatoms, the chain confines electrons belonging to surface states of pristine InAs(111)A [16]. The resulting quantized states indicate clear-cut quantum-particle-in-a-box behavior. In a simple model, we describe the electron confinement in our chains in terms of a 1D potential well of dimension L . The energy of its quantized states is

$$E_n = \frac{\hbar^2 k_n^2}{2m^*} = \frac{\hbar^2}{2m^*} \left(\frac{\pi}{L} \right)^2 n^2, \quad n = 1, 2, 3, \dots, \quad (1)$$

with k_n denoting the wave vector of the n th state and m^* the effective electron mass. The energy scales with the square of quantum number n as indicated by the blue bars in Fig. 1(b).

The In₃₀ chain in Fig. 1(a) can be rearranged to form a hexagon-shaped In₃₀ ring with the same interatomic spacing of $\sqrt{3}a'$, see Fig. 1(c). To a first approximation, we neglect the effect of the hexagonal shape and treat the problem as a circular ring of circumference $L = 2\pi R$. The expected eigenstate energies are

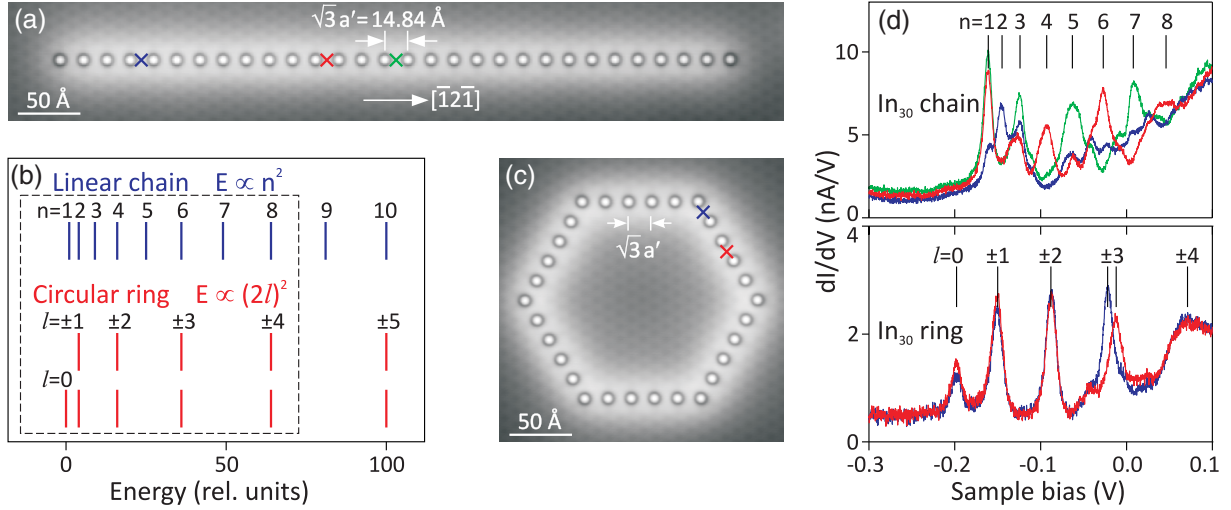


FIG. 1. (a) STM topography image (100 pA, 100 mV) of a linear In_{30} chain on $\text{InAs}(111)A$, interatomic spacing: $\sqrt{3}a' = 14.84 \text{ \AA}$ with a' the surface lattice constant of the 2×2 In-vacancy reconstruction. (b) Schematic level structure of free electrons confined in a linear chain (blue bars) and a circular ring (red bars) illustrating the energy scaling according to Eqs. (1) and (2) in the main text. (c) STM topography image (100 pA, 100 mV) of a hexagonal In_{30} ring with the same interatomic spacing of $\sqrt{3}a'$ as in (a). (d) (Upper) Conductance spectra taken along the linear chain at the tip positions indicated in (a); eight dI/dV peaks are observed, signifying the chain-confined states with quantum number $n = 1-8$. (Lower) Conductance spectra taken along the hexagonal ring at the tip positions indicated in (c); a reduced number of dI/dV peaks is observed, signifying the ring-confined states with quantum number of angular momentum $l = 0, \pm 1, \pm 2, \pm 3$, and ± 4 . The $l = \pm 3$ degeneracy is lifted as a result of the hexagonal ring shape. The dashed box in (b) highlights the experimentally observed states in (d).

$$E_l = \frac{\hbar^2 l^2}{2m^* R^2} = \frac{\hbar^2}{2m^*} \left(\frac{\pi}{L}\right)^2 (2l)^2, \quad l = 0, \pm 1, \pm 2, \pm 3, \dots \quad (2)$$

with R as the radius and l as the quantum number of angular momentum [15]. The ground state with $l = 0$ is a singlet, whereas excited states with finite angular momentum are doubly degenerate, as depicted by the red bars in Fig. 1(b). Provided that our model qualitatively describes the real structures in Figs. 1(a) and 1(c), one would expect to observe a reduced number of conductance peaks for the ring as compared to the chain.

To verify this, Fig. 1(d) compares conductance spectra of the linear In_{30} chain and the In_{30} ring recorded with the STM tip fixed at the positions marked in Figs. 1(a) and 1(c). Starting with the chain [upper panel in Fig. 1(d)], eight discrete conductance peaks are observed in the bias range from -0.3 to 0.1 V, equivalent to an energy range from 0.3 eV below the Fermi level of the InAs surface (at sample bias $V = 0$) to 0.1 eV above the Fermi level. These conductance peaks signify the chain-confined states with $n = 1-8$. Spatial conductance maps recorded at the respective peak energies reveal squared wave functions with n lobes and $(n - 1)$ nodes (see Supplemental Material Fig. S1 [21]) as we observed previously for chains with the shortest possible interatomic spacing of $a' = 8.57 \text{ \AA}$ [16]. It is noted at this point that the confinement is primarily determined by the length of the chain. The actual interatomic spacing—varied within the range of $a'-3a'$ in the

present work—does not affect the experimentally observed $E(k)$ dispersion; it merely causes a rigid (presumably electrostatic) shift in the level energies (see Supplemental Material Fig. S2 [21]).

Regarding the In_{30} ring [lower panel of Fig. 1(d)], we find that the number of conductance peaks is indeed reduced, in agreement with the predicted level scheme in Fig. 1(b). Following the level assignment given in the scheme, we observe the ground state with $l = 0$ and the excited states with $l = \pm 1, \pm 2, \pm 3$, and ± 4 within the energy range probed in the measurement. It is noted that, for hexagonal rings of different size (not shown in Fig. 1), the measured energies scale as $(l/R)^2$ (see Supplemental Material Fig. S3 [21]) indicating that Eq. (2) captures the qualitative details of the level structure. Nevertheless, of particular interest is the ~ 10 mV splitting of the eigenstate with $l = \pm 3$, which clearly goes beyond the first-order approximation of confinement in a circular ring. The splitting highlights the effect of the corner sites: the wave functions associated with $l = \pm 3$ have $2|l| = 6$ lobes so that their positions can be in perfect registry either with the corners or the sides of the hexagon. This circumstance lifts the degeneracy of the $l = \pm 3$ state because the confining potential is enhanced at the corners compared to the sides of the hexagon [23]. As a consequence, the component localized at the corners is lower in energy (blue spectrum) than that localized at the sides (red spectrum). These observations illustrate the general principle of quantum mechanics that symmetry lowering causes degeneracy lifting.

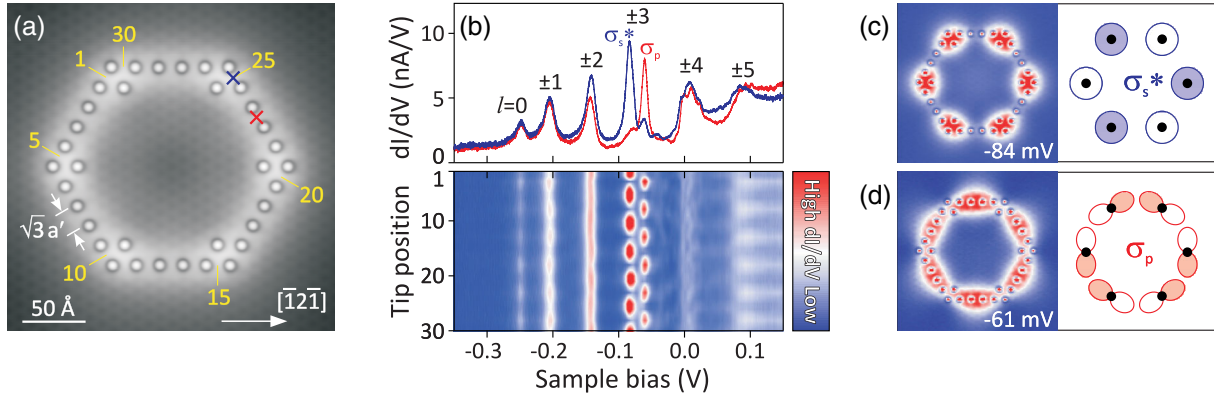


FIG. 2. (a) STM topography image (100 pA, 100 mV) of an In_{36} ring having six auxiliary In adatoms to enhance the confinement at the corners. (b) (Upper) Conductance spectra taken at the tip positions marked in (a) revealing the confined states with $l = 0$ to ± 5 ; the splitting at $l = \pm 3$ is more than twice the splitting observed for the bare In_{30} ring in Fig. 1. (Lower) Conductance map composed of 30 spectra consecutively recorded at the tip positions numbered anticlockwise in (a), the $l = \pm 3$ component at lower (higher) energy is detected at the corners (sides) of the hexagon. (c) Spatial conductance map (left) recorded for the $l = \pm 3$ component at lower energy revealing that the lobe structure of the confined wave function is equivalent to an antibonding state of s orbital character (σ_s^*), as illustrated by the scheme on the right. (d) As in (c) but recorded for the component at higher energy, the lobe structure is equivalent to a bonding state of p orbital character (σ_p).

The observed level splitting (degeneracy lifting) can be understood in analogy to the occurrence of a gap predicted for electrons in a 1D periodic potential. The effect becomes more obvious when the potential modulation is further enhanced by adding auxiliary adatoms at the corners, see Fig. 2(a). The obtained conductance spectra in Fig. 2(b) (upper panel) are qualitatively similar to those of the bare In_{30} ring in Fig. 1(d); however, they indicate a significantly larger splitting of the $l = \pm 3$ state, $\Delta(\pm 3) = 23$ mV. The conductance map in the lower panel of Fig. 2(b) is composed of 30 spectra consecutively recorded at the tip positions numbered anticlockwise in Fig. 2(a), clearly showing that the $l = \pm 3$ component at lower (higher) energy is detected at the corners (sides) of the hexagon. Consistently, the corresponding spatial conductance maps [Figs. 2(c) and 2(d)] reveal that the lobes of the confined wave function are centered at the corners for the component at lower energy (implying stronger binding), while they are centered in between of the corners for the component at higher energy (weaker binding). The corners can be viewed as *artificial* atoms (sites of enhanced confinement) coupled through the straight sides of the hexagonal ring structure.

To further rationalize the observed energy splitting [Fig. 2(b)] and the confined wave functions [Figs. 2(c) and 2(d)], we draw an analogy to the case of electrons in a 1D periodic potential, where energy gaps occur for wave vectors equal to half a reciprocal lattice vector [24]: first considering the lowest-lying energy gap, the state at the lower band gap edge is of fully antibonding s orbital character (σ_s^*), whereas the state at the upper band gap edge is of fully bonding p orbital character (σ_p). Indeed, the spatial conductance maps at $l = \pm 3$ are consistent with the expected wave function symmetry because the state at

lower energy [Fig. 2(c)] is centered at the artificial atoms and has nodes in between (σ_s^*), while the state at higher energy [Fig. 2(d)] has nodes at the atomic positions and lobes in between (σ_p). Returning to the 1D potential case, higher-lying energy gaps occur at wave vectors associated with larger reciprocal lattice vectors. Likewise, we expect energy splittings in our rings also for states with $l = \pm 6, \pm 9, \pm 12, \dots$ for which the number of wave function lobes (nodes) is a multiple of 6. States of all other quantum numbers are expected to show no splitting. This behavior is confirmed by a simple model considering the matching between the probability density of a confined state and a perturbation potential of hexagonal symmetry (see Supplemental Material Sec. IV [21]).

Finally, to access states of higher quantum number l , we assembled an enlarged ring composed of an increased number of atoms [see the In_{78} structure in Fig. 3(a) (interatomic spacing $a' = 8.57$ Å)]. The larger circumference and the enhanced confinement lead to a reduced energy level spacing. In addition, we accomplished the inverted case of potential modification by removing corner atoms from the ring. As a consequence, the potential is reduced at the corners and the artificial (now longish) atoms are now given by the remaining 13 atomic chains, which are separated by the vacant atomic sites at the corners. States of quantum numbers up to ± 9 can be readily resolved as documented by the conductance spectra in Fig. 3(b). Because of the reduced level spacing, the ground state ($l = 0$) is not resolved as a separate peak; it merges into the broadened low-energy edge of the $l = \pm 1$ state. Closer inspection of the spectra reveals a total of three splittings $\Delta(l)$ at $l = \pm 3$ (~ 6 mV), ± 6 (~ 12 mV), and ± 9 (~ 17 mV), respectively, in agreement with the

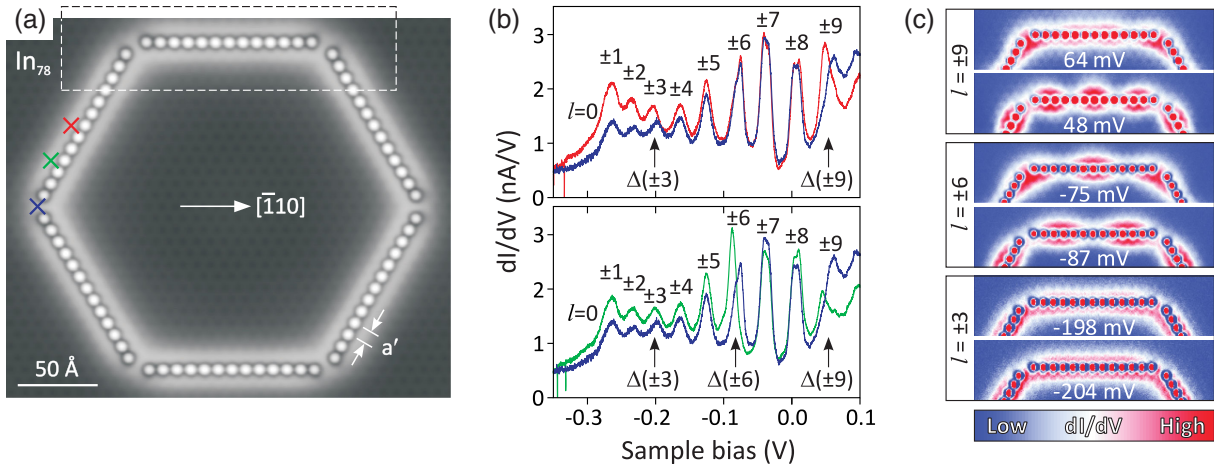


FIG. 3. (a) STM topography image (100 pA, -1 V) of an In_{78} ring with an interatomic spacing of $a' = 8.57$ Å and a vacant atomic site at each corner. (b) Conductance spectra taken at the tip positions indicated in (a) revealing confined states with an angular momentum quantum number of up to $l = \pm 9$; due to the reduced level spacing the ground state ($l = 0$) is not resolved as a separate peak. Three splittings $\Delta(l)$ at $l = \pm 3$ (~ 6 mV), ± 6 (~ 12 mV), and ± 9 (~ 17 mV) are observed. The higher-energy component of each split state is associated with the corners (i.e., inverted compared to the cases in Figs. 1 and 2) because the vacant atomic sites reduce the confinement at the corners. (c) Conductance maps of the split states recorded in the close-up region marked by the dashed box in (a). The wave functions have $2|l|$ lobes and the lobes (nodes) of the component at higher (lower) energy are in registry with the corners. For the split state at $l = \pm 3$ the lobe structure is not resolved because of the reduced level spacing.

expectations discussed above. For the corresponding squared wave functions, we observe a total of $2|l|$ lobes as inferred from the close-up conductance maps in Fig. 3(c). At a given $|l|$, the lobes (nodes) of the wave function at higher (lower) energy are in registry with the corners, which is consistent with the weaker binding in those locations. These features are clearly observed in the conductance maps for $l = \pm 6$ and $l = \pm 9$, whereas they are less obvious for the case of the lower quantum number $l = \pm 3$. This limitation is again a consequence of the reduced level spacing resulting from the enlarged circumference of the ring.

In conclusion, our results show that atom manipulation on the $\text{InAs}(111)\text{A}$ surface allows one to engineer atomically precise quantum rings. These rings exhibit quantized states that emerge from the electrostatic confinement of surface-state electrons [16]. The energy spectrum of the quantized states is qualitatively consistent with 1D confinement along a closed loop. The hexagonal ring shape (predefined by the surface symmetry) leads to a periodic potential modulation that weakly perturbs the states. The result of this perturbation can be understood in analogy to the behavior of electrons in a 1D periodic potential. The modulation of the potential can be enhanced or even inverted by further adding or removing individual atoms with the STM tip. We anticipate that the present approach can be extended to construct two-dimensional artificial lattices (known as “quantum materials”) [25], some of which have been created recently by atom manipulation on metal surfaces [26–28]. Constructing artificial lattices on a semiconductor surface has obvious advantages because screening effects are

reduced as compared to metals. This allows for a tunable electrostatic confinement of carriers by charged (and repositionable) point defects and enables the addressability of STM-generated structures by external gate electrodes [29].

Financial support by the Deutsche Forschungsgemeinschaft (FO 362/4-2) is gratefully acknowledged. The authors like to thank Steven C. Erwin, Randall M. Feenstra, and Stefan Ludwig for helpful and inspiring discussions.

- [1] Y. Aharonov and D. Bohm, *Phys. Rev.* **115**, 485 (1959).
- [2] R. A. Webb, S. Washburn, C. P. Umbach, and R. B. Laibowitz, *Phys. Rev. Lett.* **54**, 2696 (1985).
- [3] J. Appenzeller, Th. Schäpers, H. Hardtdegen, B. Lengeler, and H. Lüth, *Phys. Rev. B* **51**, 4336 (1995).
- [4] A. Yacoby, M. Heiblum, D. Mahalu, and H. Shtrikman, *Phys. Rev. Lett.* **74**, 4047 (1995).
- [5] A. Fuhrer, S. Lüscher, T. Ihn, T. Heinzel, K. Ensslin, W. Wegscheider, and M. Bichler, *Nature (London)* **413**, 822 (2001).
- [6] M. Büttiker, Y. Imry, and R. Landauer, *Phys. Lett.* **96A**, 365 (1983).
- [7] R. Landauer and M. Büttiker, *Phys. Rev. Lett.* **54**, 2049 (1985).
- [8] L. P. Lévy, G. Dolan, J. Dunsmuir, and H. Bouchiat, *Phys. Rev. Lett.* **64**, 2074 (1990).
- [9] D. Mailly, C. Chapelier, and A. Benoit, *Phys. Rev. Lett.* **70**, 2020 (1993).
- [10] U. F. Keyser, C. Fühner, S. Borck, R. J. Haug, M. Bichler, G. Abstreiter, and W. Wegscheider, *Phys. Rev. Lett.* **90**, 196601 (2003).

- [11] P. Földi, B. Molnár, M. G. Benedict, and F. M. Peeters, *Phys. Rev. B* **71**, 033309 (2005).
- [12] S. K. Maiti *Phys. Lett. A* **373**, 4470 (2009).
- [13] A. Lorke, R. J. Luyken, A. O. Govorov, and J. P. Kotthaus, *Phys. Rev. Lett.* **84**, 2223 (2000).
- [14] J. A. Stroschio and D. M. Eigler, *Science* **254**, 1319 (1991).
- [15] For review see, e.g., A. G. Aronov and Y. V. Sharvin, *Rev. Mod. Phys.* **59**, 755 (1987); S. Viefers, P. Koskinen, P. Singha Deo, and M. Manninen, *Physica (Amsterdam)* **21E**, 1 (2004).
- [16] S. Fölsch, J. Martínez-Blanco, J. Yang, K. Kanisawa, and S. C. Erwin, *Nat. Nanotechnol.* **9**, 505 (2014).
- [17] K. Kanisawa and T. Fujisawa, *Hyomen Kagaku* **29**, 747 (2008).
- [18] J. Yang, S. C. Erwin, K. Kanisawa, C. Nacci, and S. Fölsch, *Nano Lett.* **11**, 2486 (2011).
- [19] J. Yang, C. Nacci, J. Martínez-Blanco, K. Kanisawa, and S. Fölsch, *J. Phys. Condens. Matter* **24**, 354008 (2012).
- [20] Y. Pan, K. Kanisawa, and S. Fölsch, *J. Vac. Sci. Technol. B* **35**, 04F102 (2017).
- [21] See Supplemental Material at <http://link.aps.org/supplemental/10.1103/PhysRevLett.123.066801> for Figs. S1–S4, which also includes Refs. [15,22]. Figure S3 shows the size-dependent scaling behavior for hexagonal rings with an interatomic spacing of $s = 2 a'$. The effective radius is $R = sN/(2\pi)$ with N denoting the number of atoms.
- [22] R. M. Feenstra, Y. Dong, M. P. Semtsiv, and W. T. Masselink, *Nanotechnology* **18**, 044015 (2007).
- [23] The spatial density of the positively charged adatoms is locally larger at the corners than at the straight sides of the hexagon, thus inducing enhanced confinement at the corners compared to the sides.
- [24] N. W. Ashcroft and N. D. Mermin, *Solid State Physics* (Saunders College Publishing, New York, 1976).
- [25] For review, see M. Polini, F. Guinea, M. Lewenstein, H. C. Manoharan, and V. Pellegrini, *Nat. Nanotechnol.* **8**, 625 (2013).
- [26] K. K. Gomes, W. Mar, W. Ko, F. Guinea, and H. C. Manoharan, *Nature (London)* **483**, 306 (2012).
- [27] R. Drost, T. Ojanen, A. Harju, and P. Liljeroth, *Nat. Phys.* **13**, 668 (2017).
- [28] M. R. Slot, S. N. Kempkes, E. J. Knol, W. M. J. van Weerdenburg, J. J. van den Broeke, D. Wegner, D. Vanmaekelbergh, A. A. Khajetoorians, C. Morais Smith, and I. Swart, *Phys. Rev. X* **9**, 011009 (2019).
- [29] M. Fuechsle, J. A. Miwa, S. Mahapatra, H. Ryu, S. Lee, O. Warschkow, L. C. L. Hollenberg, G. Klimeck, and M. Y. Simmons, *Nat. Nanotechnol.* **7**, 242 (2012).